

Synthesis, Radiofluorination, and In Vitro Evaluation of Pyrazolo[1,5-*a*]pyridine-Based Dopamine D₄ Receptor Ligands: Discovery of an Inverse Agonist Radioligand for PET

Olaf Prante,^{*,†} Rainer Tietze,[†] Carsten Hocke,[†] Stefan Löber,[‡] Harald Hübner,[‡] Torsten Kuwert,[†] and Peter Gmeiner[‡]

Laboratory of Molecular Imaging, Clinic of Nuclear Medicine, Friedrich-Alexander University, 91054 Erlangen, Germany, and Department of Chemistry and Pharmacy, Emil Fischer Center, Friedrich-Alexander University, 91052 Erlangen, Germany

Received November 2, 2007

A series of fluoro-substituted analogs structurally derived from the aminomethyl-substituted pyrazolo[1,5-*a*]pyridine lead compounds **9** (FAUC 113) and **10** (FAUC 213) were synthesized and evaluated as high-affinity D₄ receptor (D₄R) ligands (**3a–3h**, K_i = 1.3–28 nM). The *para*-fluoroethoxy-substituted derivatives **3f** and **3h** revealed an outstanding D₄ subtype selectivity of more than 3 orders of magnitude over both congeners D₂ and D₃ combined with inverse agonism at D₄R. The corresponding ¹⁸F-labeled radioligands revealed high serum stability in vitro and log *P* values of 2–3. In vitro rat brain autoradiography showed specific binding of [¹⁸F]**3h** in distinct brain regions, including the gyrus dentate of the hippocampus, that were inhibited by both eticlopride (65–80%) and the selective D₄R antagonist **10** (78–93%). The observed binding pattern was mainly consistent with the known D₄R distribution in the rat brain. Thus, [¹⁸F]**3h** (FAUC F41) represents a potential radioligand for studying the D₄R in vivo by positron emission tomography (PET).

Introduction

The subfamily of D₂-like dopamine receptors includes the D₂-, D₃-, and D₄-receptor subtypes (D₂R, D₃R, D₄R) and mediates the action of dopamine in the brain by inhibition of adenylate cyclase activity. Dopamine receptor subtypes differ with regard to their distribution within the brain and their density.¹ D₂Rs are highly expressed in the striatum, whereas D₃Rs are predominantly located in the mesocorticolimbic system, especially in the nucleus accumbens and the Islands of Calleja. D₃R density is, however, lower than that of the D₂Rs.^{2,3} The D₄R was cloned from a genomic library in 1991.⁴ Some evidence points to its preferential expression in the prefrontal cortex and limbic areas such as the hippocampus, the amygdala, the thalamic reticular nucleus, and the hypothalamus of the rat brain.^{5–8} Immunohistological studies using D₄ antireceptor antisera or sequence-specific D₄R antibodies have, however, yielded some discrepant results. Khan et al. found highest expression in cortical areas and the hippocampus of the rat brain,⁸ whereas Ariano et al. found predominant expression of the rat D₄ receptor in the prefrontal cortex.⁵ Defagot et al. supplemented these results by reporting highest D₄ positive antibody staining in the prefrontal cortex followed by hippocampus, cortex, entorhinal cortex, and amygdala.⁷ Recently, Noaín et al. reinvestigated the D₄R expression pattern in the brain of bacterial artificial chromosome (BAC) transgenic mice that express enhanced green fluorescent protein (EGFP) under the transcriptional control of the mouse D₄ receptor gene, confirming predominant expression in the prefrontal cortex of such animals.⁹

Moreover, using autoradiography with the D₄-selective radioligand [³H]NGD 94-1,^{10,11} the apparently low D₄ receptor densities have been reported to range between 9 and 30 fmol/mg in the entorhinal cortex, septum, and hippocampus of the rat brain.⁶ However, this D₄ receptor distribution was not consistent with autoradiography studies, in which the number

of binding sites defined with [³H]raclopride (D₂/D₃ antagonist) were subtracted from total binding of [³H]nemonapride.^{12,13} Therefore, some uncertainties on D₄R expression still prevail, in particular, due to the limited availability of a selective D₄ receptor radioligand with high affinity and selectivity over the other dopamine receptor subtypes.¹⁴ Due to the above-described methodological problems, evidence on the precise distribution and regulatory mechanisms of the D₄R in health and disease is scarce. It has been implicated in novelty seeking and libidinous behavior that is influenced by D₄R agonists inducing the release of oxytocin.^{15–17} Furthermore, the disturbance of neural networks involving the D₄R has been assumed in various neurobehavioral and psychiatric disorders, such as attention-deficit hyperactivity disorder (ADHD^a) and schizophrenia.^{18–20}

Molecular imaging with positron emission tomography (PET) is in principle suited to gain deeper insight into the physiological and pathophysiological role of the D₄R also in the human.²¹ However, its use for this purpose has been obviated by the lack of bioavailable D₄ receptor selective radioligands, although recent progress in the development of dopamine receptor subtype-selective ligands has been achieved.^{22,23} Recently, newly developed compounds with high affinity for D₄ receptors combined with potent serotonin reuptake inhibition, such as Lu 35-138²⁴ and others,^{25,26} have been described. However, lacking high specificity toward D₄R would prevent these ligands from serving as lead compounds for the development of PET analogs. In the past, various attempts have been reported toward the development of ¹⁸F- and ¹¹C-labeled D₄ receptor radioligands, including [¹¹C]SDZ-GLC756,²⁷ methoxybenzamide derivatives,^{28,29} SB-235753³⁰ or ¹⁸F-labeled pyrrolo[2,3-*b*]pyridines.^{31,32} However, none of these radioligands has as yet been proven

* To whom correspondence should be addressed. Phone: +49 9131 8544440. Fax: +49 9131 8534325. E-mail: olaf.prante@uk-erlangen.de.

[†] Laboratory of Molecular Imaging, Clinic of Nuclear Medicine.

[‡] Department of Chemistry and Pharmacy.

^a Abbreviations: ADHD, attention-deficit hyperactivity disorder; cLogP, calculated logarithm of distribution coefficient between octanol and water; CM, central medial thalamic nucleus; CX, cortex; EOS, end of synthesis; HC, hippocampus; HRMS, high-resolution mass spectrometry; HT, hypothalamus; MHb, medial habenular nucleus, PBS, phosphate-buffered saline; PET, positron emission tomography; RCY, radiochemical yield; SD, standard deviation; s, septum; ST, striatum.

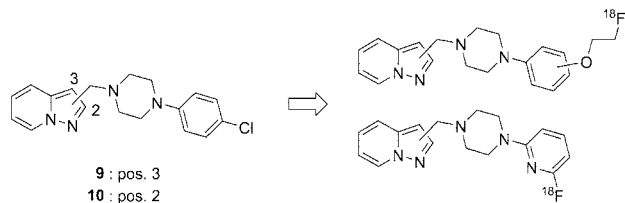
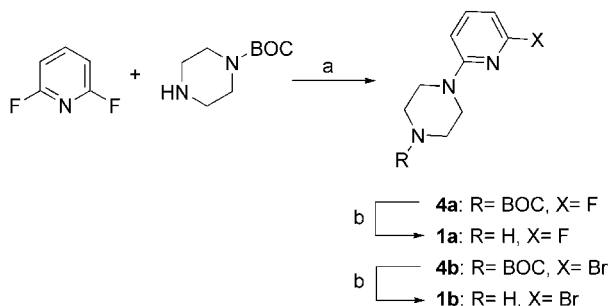


Figure 1. Development of ¹⁸F-labeled D₄ radioligands.

Scheme 1. Synthesis of (6-Halopyridin-2-yl)piperazines **1a,b**^a



^a Reaction conditions: (a) triethylamine, DMF, reflux, 20 h; (b) dioxane/HCl (1:1), 2 h.

suitable for PET studies due either to low specific binding in vivo or undesirable pharmacological properties, such as rapid metabolism.

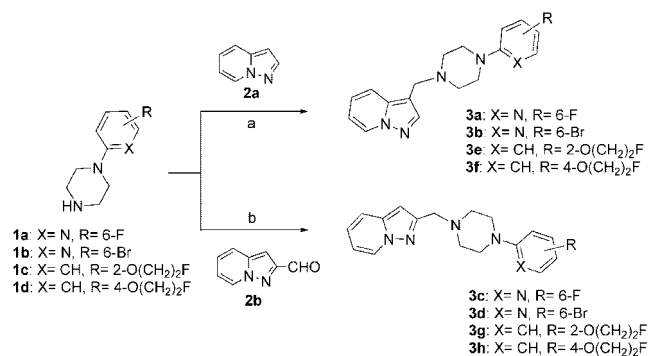
As a result of our previous drug discovery and structure–activity relationship (SAR) studies on selective dopamine D₄ receptor–ligands, we developed the pyrazolo[1,5-*a*]pyridine derivatives **9** (FAUC 113)³³ and **10** (FAUC 213),³⁴ bearing the (4-chlorophenyl)piperazinylmethyl moiety in 3- and 2-position of the pyrazolo[1,5-*a*]pyridine core, respectively, as high-affinity dopamine D₄ receptor–ligands with superior subtype selectivity.^{33–36} Interestingly, **9** has been found to show partial D₄R agonism, whereas **10** revealed complete D₄R antagonism in a cell-based mitogenesis assay using [³H]quinpirole as a reference.³⁴ Moreover, **10** exhibited atypical antipsychotic properties in animal models of behavioral neurobiology.³⁶ On the basis of these previous findings, we chose **9** and **10** as interesting lead compounds for the development of ¹⁸F-labeled PET ligands. In this study, we aimed at introducing a (2-fluoroethoxy)phenyl or a (6-fluoropyridin-2-yl)phenyl group into the positions 2 or 3 of the pyrazolo[1,5-*a*]pyridine framework, replacing the 4-chlorophenyl moiety of the lead structure, to develop fluoro-substituted candidates that also should be accessible by efficient ¹⁸F-labeling techniques (Figure 1).

Extending our recent work on the development of D₃- and D₄-selective radioligands,^{37–40} we herein describe the synthesis, in vitro characterization, and ¹⁸F-labeling of a new series of D₄ receptor radioligands derived from the lead compounds **9** and **10**. Finally, one promising D₄ radioligand with improved D₄ subtype selectivity was chosen for in vitro brain autoradiography to assess its in vivo properties as a D₄ PET radioligand candidate.

Results and Discussions

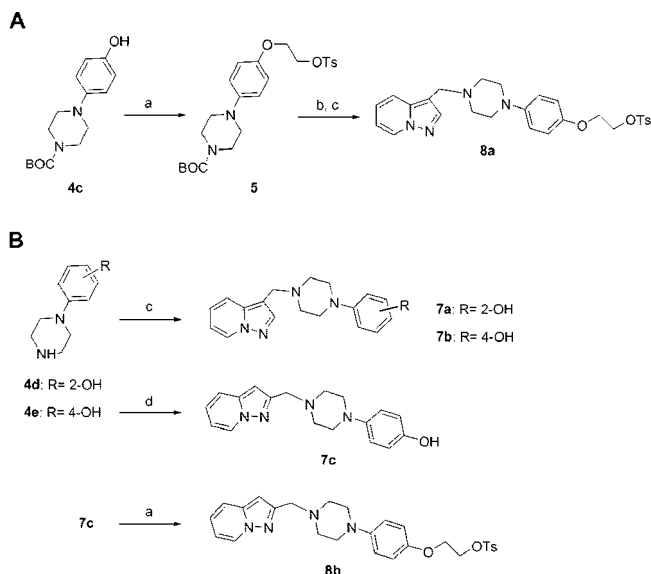
Chemistry. Our strategy toward the preparation of this new series of test ligands was based on the availability of the arylpiperazines **1a–d**. Reaction of 2,6-difluoropyridine and 1-Boc-piperazine under basic conditions in DMF and subsequent cleavage of the *t*-butyl carbamate (**4a**) readily afforded (6-fluoropyridin-2-yl)piperazine (**1a**; Scheme 1). The corresponding 6-bromo derivative **1b** was prepared similarly starting from the

Scheme 2. Syntheses of **3a–3h**^a



^a Reaction conditions: (a) CH₂O, AcOH, CH₂Cl₂, rt, 24 h; (b) Na(OAc)₃BH, CH₂Cl₂, rt, 24 h.

Scheme 3. Synthesis of the Labeling Precursor compounds **7a**, **7b**, **8a**, and **8b**^a

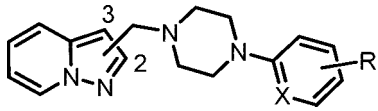


^a Reaction conditions: (a) C₂H₄(OTs)₂, K₂CO₃, CH₃CN, reflux, 8 h; (b) dioxane/HCl (1:1); (c) **2a**, CH₂O, AcOH, CH₂Cl₂, rt, 24 h; (d) **2b**, Na(OAc)₃BH, CH₂Cl₂, rt, 24 h.

commercially available *N*-Boc-protected pyridinylpiperazine **4b**. The *ortho*- and *para*-(fluoroethoxy)phenyl piperazines **1c** and **1d** were synthesized as described recently.³⁹

With the arylpiperazines **1a–1d** in hand, we prepared a new series of 6-halopyridin-2-yl-, *o*-, and *p*-(2-fluoroethoxy)phenyl-substituted derivatives of **9** and **10** by employing Mannich reaction with **2a** and reductive amination with pyrazolo[1,5-*a*]pyridine-2-carbaldehyde (**2b**) in the presence of Na(OAc)₃BH, respectively, as depicted in Scheme 2. Following these reaction pathways, a set of 3-substituted pyrazolo[1,5-*a*]pyridines (**3a**, **3b**, **3c**, and **3f** (Scheme 2); **7a**, **7b** (Scheme 3b) was obtained in 16–90% yield, and the corresponding series of 2-substituted target compounds (**3c**, **3d**, **3g**, and **3h**) was achieved in a yield of 29–57%. The obtained series of compounds included the reference compounds of the aspired radiolabeled analogs (**3a**, **3c**, **3e–h**), the ¹⁸F-labeling precursors for aromatic ¹⁸F-for-Br substitution using *ortho*-bromo-substituted pyridinyl compounds **3b** and **3d**, and precursor compounds **7a** and **7b** suitable for ¹⁸F-ethylation using [¹⁸F]fluoroethyltosylate.

Receptor Binding Experiments. After purification by flash chromatography and confirmation of chemical purity by LC/MS, HPLC, and HRMS, the test compounds **3a–h** were

Table 1. Binding Affinities of the Fluorinated Target Compounds **3a**, **3c**, and **3e–h** to the Human Dopamine Receptor Subtypes D_{2long}, D_{2short}, D₃, and D₄, the Porcine D₁ Receptor, as Well as the Porcine 5-HT_{1A}, 5-HT₂, and α_1 Receptors in Comparison with the Labeling Precursors **3b**, **3d**, **7a**, and **7b** and the Reference Compounds **9** and **10**


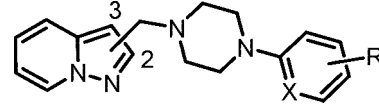
				K _i values ^a (nM ± SEM)							
cmpd	pos.	X	R	[³ H]spiperone				[³ H]SCH 23990	[³ H]8-OH-DPAT	[³ H]ketanserin	[³ H]prazosin
				D _{2long}	D _{2short}	D ₃	D _{4.4}	D ₁	5-HT _{1A}	5-HT ₂	α_1
3a	3	N	6-F	330 ± 0	220 ± 65	590 ± 60	8.8 ± 1.0	7300 ± 1300	290 ± 85	5400 ± 250	87 ± 9.0
3b	3	N	6-Br	210 ± 30	150 ± 25	410 ± 55	2.6 ± 0.8	3900 ± 2600	120 ± 36	1200 ± 300	21 ± 1.0
3c	2	N	6-F	3400 ± 1300	1700 ± 790	3400 ± 600	24 ± 1.5	30000 ± 4500	1200 ± 50	9700 ± 250	910 ± 200
3d	2	N	6-Br	880 ± 95	550 ± 75	930 ± 75	7.9 ± 0.5	18000 ± 4500	360 ± 0	4400 ± 650	240 ± 0
3e	3	CH	2-O(CH ₂) ₂ F	150 ± 26	180 ± 34	320 ± 27	1.6 ± 0.1	2500 ± 87	120 ± 5.0	2900 ± 250	5.4 ± 0.4
3f	3	CH	4-O(CH ₂) ₂ F	66000 ± 13000	79000 ± 18000	8700 ± 2700	28 ± 0.5	33000 ± 5000	13000 ± 0	14000 ± 1500	4500 ± 380
3g	2	CH	2-O(CH ₂) ₂ F	46 ± 8.5	79 ± 19	940 ± 160	1.3 ± 0.1	4800 ± 100	5700 ± 1200	13000 ± 10000	40 ± 9.5
3h	2	CH	4-O(CH ₂) ₂ F	30000 ± 1000	50000 ± 5500	15000 ± 1000	13 ± 0.5	29000 ± 2500	1400 ± 200	5500 ± 1600	4100 ± 0
7a	3	CH	2-OH	4500 ± 450	4700 ± 1200	2200 ± 0	44 ± 15	2800 ± 250	680 ± 430	1500 ± 150	26 ± 2.5
7b	3	CH	4-OH	6100 ± 550	87000 ± 1300	3400 ± 250	20 ± 1.5	9900 ± 100	12000 ± 1500	24700 ± 700	82 ± 7.0
9	3	CH	4-Cl	2900 ± 2950	2200 ± 670	4500 ± 360	5.8 ± 0.9	2800 ± 50	1400 ± 130	380 ± 140	240 ± 5.0
10	2	CH	4-Cl	3400 ± 450	6300 ± 1900	5300 ± 720	2.2 ± 0.2	5500 ± 1300	1700 ± 360	900 ± 200	270 ± 13

^a K_i values are expressed as mean ± SEM of 2–8 experiments, each performed in triplicate.

subjected to receptor binding studies to determine their ability to displace [³H]spiperone from the cloned human dopamine receptors D_{2long}, D_{2short},⁴¹ D₃,⁴² and D₄⁴³ being stably expressed in Chinese hamster ovary (CHO) cells.⁴⁴ In addition, the receptor affinity profile was extended by the related biogenic amine receptors 5-HT_{1A}, 5-HT₂, and α_1 that were measured utilizing porcine cortical membranes and the selective radioligands [³H]8-OH-DPAT, [³H]ketanserin, and [³H]prazosin, respectively. For straight comparison of the binding data, the lead compounds **9** and **10** were investigated under identical experimental conditions. The results of the receptor binding studies are presented in Table 1.

In fact, the dopamine receptor binding profiles of all compounds indicated poor affinities for the D₁, D₂, and D₃ subtypes and highest affinity for the D₄ receptor subtype with K_i values ranging from 1.3 to 44 nM. The results for the 6-halopyridinyl derivatives **3a–3d** showed higher D₄ affinities for the bromo-substituted compounds (**3b**, **3d**) in comparison with the corresponding fluoro derivatives (**3a**, **3c**; Table 1). Comparison of the D₄ binding data among each test compound revealed significantly higher D₄ receptor affinities in the low nanomolar range (1–2 nM) for derivatives bearing a fluoroethoxy substituent in *ortho*-position of the phenylpiperazinyl moiety (**3e**, **3g**). However, this encouraging result is accompanied by an increased affinity to the dopamine D₂ receptor and to the interfering α_1 receptor (Table 1, **3e** and **3g**). Interestingly, the corresponding *para*-fluoroethoxy derivatives **3f** and **3h** displayed a similar receptor binding profile with a K_i for the D₄ receptor of 28 nM and 13 nM, respectively, high dopamine receptor subtype selectivities (D₂/D₄ > 2000), and a substantial low α_1 affinity (>4000 nM, Table 1). These findings are consistent with our recent results on the comparison of *ortho*- and *para*-fluoroethoxyphenyl-substituted 5-cyano indole derivatives.³⁹

Looking at dopamine receptor subtype selectivities in more detail (Table 2), it is obvious that the pyridinyl compounds **3a** and **3c** and the *ortho*-fluoroethoxyphenyl analogs **3e** and **3g** suffer from low subtype selectivities when compared to the lead structures **9** and **10**. Contrary, the corresponding analogs bearing a *para*-fluoroethoxyphenyl group (**3f** and **3h**) revealed excellent dopamine D₄/D₂ receptor subtype selectivities of >2300 that were even superior to that of the lead compounds **9** and **10**.

Table 2. D₄ Subtype Selectivities within the Dopamine D₂ Receptor Family of the Fluorinated Target Compounds **3a**, **3c**, and **3e–h** in Comparison with the Reference Compounds **9** and **10**


				D ₄ R subtype selectivities ^a		
cmpd	pos.	X	R	D _{2long} /D _{4.4}	D _{2short} /D _{4.4}	D ₃ /D _{4.4}
3a	3	N	6-F	38	25	67
3e	3	CH	2-O(CH ₂) ₂ F	94	112	200
3f	3	CH	4-O(CH ₂) ₂ F	2360	2821	311
9	3	CH	4-Cl	500	379	776
3c	2	N	6-F	142	71	142
3g	2	CH	2-O(CH ₂) ₂ F	35	61	723
3h	2	CH	4-O(CH ₂) ₂ F	2308	3846	1154
10	2	CH	4-Cl	1546	2864	2409

^a D₄ receptor subtype selectivities are expressed as the ratios K_i(D_{2long})/K_i(D_{4.4}), K_i(D_{2short})/K_i(D_{4.4}), and K_i(D₃)/K_i(D_{4.4}), using the mean K_i values from Table 1.

Within the series of *ortho*- and *para*-fluoroethoxy-substituted test compounds, there were no significant differences in the D₄/D₃ receptor subtype selectivities (Table 2). However, compound **3h** displayed a D₄/D₃ selectivity of >1100, which was comparable to that of the lead compounds **9** (780) and **10** (2400) (Table 2). In general, **3h** was characterized as a high affinity D₄ receptor ligand with an outstanding subtype selectivity preferring the D₄ receptor, a weak receptor affinity for α_1 , 5-HT_{1A}, and 5-HT₂, thus illustrating interesting *in vitro* properties that encouraged the optimization of the radiosynthesis of the ¹⁸F-labeled analog [¹⁸F]**3h**, aiming at further *in vitro* studies, such as autoradiography using rat brain slices.

In Vitro Functional Assay. Considering the marked neuropharmacological differences of the regioisomers **9** and **10**,³⁴ we aimed at extending the data on receptor affinities of our series of compounds with functional data. Agonist activation of dopamine receptors is known to increase mitogenesis in heterologously transfected cell lines that can be determined by measuring the rate of [³H]thymidine incorporation into growing cells.⁴⁵ We studied and compared the intrinsic activities of the highly D₄ selective *para*-fluoroethoxy-substituted ligands **3f** and **3h** and the *ortho* regioisomers **3e** and **3g** by measuring the rate

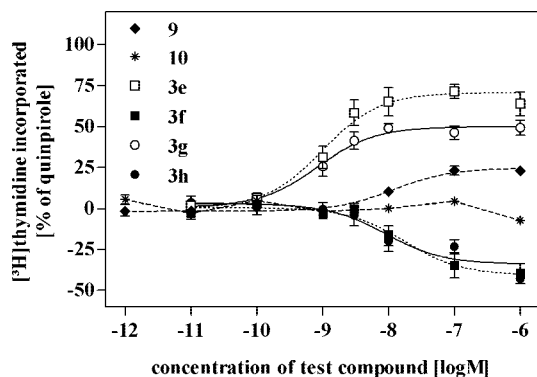


Figure 2. Intrinsic activities of **3e–h** in comparison with the reference compounds **9** (partial agonist) and **10** (neutral antagonist) derived from the D₄ stimulating effect on cellular [³H]thymidine uptake.

Table 3. Intrinsic Activity of the Pyrazolo[1,5-*a*]pyridines **3e–h**, **9**, and **10** Relative to the Reference Compound Quinpirole at the Dopamine D₄ Receptor Established by Measuring the Stimulation of Mitogenesis

	test compounds						
	quinpirole	3e	3f	3g	3h	9 ^c	10 ^c
ligand efficacy ^a	100%	71%	-41%	49%	-37%	26%	<3%
EC ₅₀ ^b (nM)	7.1	1.0	18	0.8	9.1	12	nd

^a Rate of incorporation of [³H]thymidine (in %) as a measure of mitogenic activity relative to the full agonist effect of quinpirole (100%) as the mean value of quadruplicates from 10 independent experiments. ^b EC₅₀ values are derived from the mean curves of the experiments. ^c Ref 34; nd = not determined.

of [³H]thymidine incorporation into growing CHO cells stably expressing the dopamine D_{4.2} receptor (Figure 2). When quinpirole as a full agonist reference of maximum efficacy is used, the results of the mitogenesis assay for compounds **3e** and **3g** clearly revealed partial agonism for D_{4.2}, displaying intrinsic activities of 70 and 49%, respectively, and substantial ligand potency, as summarized in Table 3. Interestingly, the mitogenesis assay demonstrated inverse agonist activity of about -40% for both *para*-substituted regioisomers **3f** and **3h**. The structurally closely related regioisomers **9** (partial agonist) and **10** (neutral antagonist)³⁴ differ from **3f** and **3h** by a 4-chlorophenylpiperazine instead of a 4-(2-fluoroethoxy)phenylpiperazine core, however, the fluoroethoxy substitution in *para*-position obviously results in a shift of the pharmacological efficacy for this class of pyrazolo[1,5-*a*]pyridine based D₄ ligands toward inverse agonism.

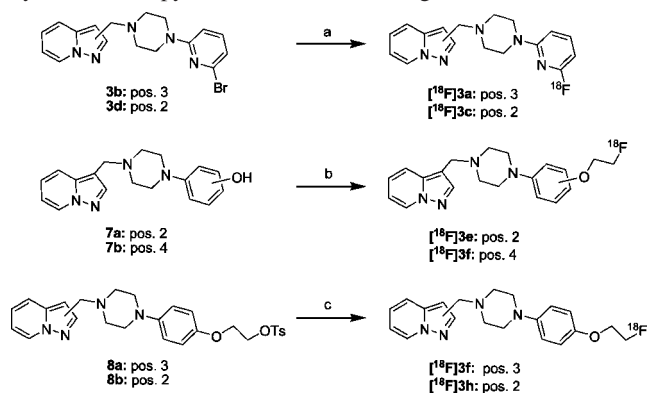
In recent years, the increased availability of recombinant and constitutively active G-protein-coupled receptor (GPCR) systems led to the discovery of the phenomenon of inverse agonism, providing evidence for the potential of GPCRs to be active in absence of agonists.⁴⁶ Based on the most simple model, GPCRs exist in a dynamic equilibrium between the active state (R*) and inactive state (R), when agonists preferentially bind to R* shifting the equilibrium toward the active conformation, and neutral antagonists display equal affinity for R* and R. In contrast, inverse agonists selectively bind to R, thereby causing a redistribution of receptor species from the active state into the inactive receptor state, which results in a decrease in constitutive activity, provided that spontaneous active states of GPCR had been present in the system.⁴⁷ Recently, a large series of typical and atypical antipsychotics was tested for D₂-like receptor activity at cells cotransfected with Gα_o.⁴⁸ The majority of compounds were determined to be D₂ and D₃ inverse agonists, whereas, notably, none was D₄ inverse agonist, although many were potent D₄ partial agonists or neutral antagonists.⁴⁸

To our knowledge, our finding that **3f** and **3h** act as inverse agonists at the D₄ receptor represents as yet the first report on this phenomenon regarding selective ligands for the D₄ receptor subtype. Although intrinsic constitutive receptor activity and inverse agonism have been frequently observed in vitro for various GPCRs, the therapeutic relevance of inverse agonist drugs as yet remains to be elucidated.^{46,49} However, the *para*-(2-fluoroethoxy)phenyl-substituted pyrazolo[1,5-*a*]pyridines **3f** and **3h** could serve as interesting lead compounds for the development of more potent D₄ inverse agonists and for studying D₄ receptor mutants in functional assays.

Clearly, the degree of inverse D₄ agonism of potential active drugs depends on the presence of an adequate degree of constitutive activity. Moreover, the level of basal activation of dopamine receptors in vivo is unclear and difficult to measure due to the presence of endogenous dopamine. However, for imaging purposes and aiming at the development of D₄ PET ligands, the level of basal activation of D₄ receptors in vivo does not play a key role for being successful because the application of PET ligands relies on the “tracer concept”, that is, the use of negligible amounts of radioactive ligands for binding studies without disturbing the dynamic receptor equilibrium significantly. One of the most important prerequisites of a suitable D₄ PET ligand is high receptor selectivity, therefore, inverse agonism could be a useful feature of a suitable D₄ PET radioligand due to the ability of such compounds to preferentially bind to the inactive state of the receptor. Thus, our notion that **3f** and **3h** act as inverse agonist D₄ ligands might be beneficial for the development of D₄ radioligands with improved functional selectivity for the inactive D₄ receptor conformation.

Radiochemistry. As a prerequisite for the radiosynthesis of the ¹⁸F-labeled analogs, we prepared the set of suitable labeling precursor compounds, as shown in Scheme 3. Starting from *N*-Boc-protected hydroxyphenylpiperazine **4c**, the tosyllethoxy group was introduced by reaction with ethylene glycol-1,2-ditosylate in the presence of potassium carbonate to afford **5** in good yields (63%), employing the protocol of Wang et al.⁵⁰ Cleavage of the piperazine nitrogen under acidic conditions provided the free amine (**6**), which was subsequently reacted with **2a** under Mannich reaction conditions to obtain the desired labeling precursor **8a** bearing a tosylate leaving group in 40% yield (Scheme 3a). Mannich reactions of **2a** with piperazines **4d** or **4e**, respectively, readily afforded the desired labeling precursor compounds **7a** and **7b** (Scheme 3b), each bearing an aromatic hydroxy group for ¹⁸F-fluoroethylation reactions by the use of [¹⁸F]fluoroethyltosylate. Furthermore, the aldehyde **2b** and the piperazine **4e** in the presence of Na(OAc)₃BH afforded intermediate **7c** that was treated with ethylene glycol-1,2-ditosylate to obtain the desired precursor compound **8b** bearing a tosylate leaving group for direct nucleophilic displacement by [¹⁸F]fluoride (Scheme 3b).

With these labeling precursors in hand, we systematically investigated the ¹⁸F-syntheses of [¹⁸F]**3a**, [¹⁸F]**3c**, [¹⁸F]**3e**, [¹⁸F]**3f**, and [¹⁸F]**3h** leading to the optimized reaction conditions presented in Table 3. Scheme 4 summarizes the various ¹⁸F-labeling reactions that were performed to obtain the respective ¹⁸F ligands. Applying typical reaction conditions for aromatic ¹⁸F-for-Br substitution to *ortho*-bromo-substituted pyridinyl derivatives (**3b** or **3d**), that is, high reaction temperature (180 °C) and long reaction time (45 min), the ¹⁸F-labeled ligands [¹⁸F]**3a** and [¹⁸F]**3c** were obtained in high radiochemical yields (RCY) of 69 and 80%, respectively (Scheme 4, Table 4). Furthermore, the [¹⁸F]fluoroethoxy-substituted radioligands [¹⁸F]**3e** and [¹⁸F]**3f** were achieved by a two-step procedure

Scheme 4. Radiosynthesis of ^{18}F -labeled Pyrazolo[1,5-*a*]pyridine Based D_4 Radioligands^a


^a Reaction conditions: (a) [^{18}F]fluoride (potassium 222 kryptate), DMSO, 180 °C, 45–60 min; (b) 2-[^{18}F]fluoroethyltosylate, sodium methanolate, DMF, 120 °C, 5 min; (c) [^{18}F]fluoride (potassium 222 kryptate), CH_3CN , 85 °C, 10 min.

consisting of the radiosynthesis of [^{18}F]fluoroethyltosylate⁵¹ and subsequent ^{18}F -ethylation of **7a** or **7b** in the presence of sodium methanolate as base (Scheme 4). The final alkylation step of this laborious labeling procedure revealed high RCYs of 92% (^{18}F]3e) and 87% (^{18}F]3f; Table 4), however, the overall synthesis time was two hours, being a major disadvantage when considering the short half-life of fluorine-18 (110 min). Utilizing the tosylate precursors **8a** and **8b** for a direct kryptate-assisted nucleophilic ^{18}F -fluorination in acetonitrile afforded the desired radioligands [^{18}F]3f and [^{18}F]3h in a straightforward reaction with a yield of 26% (nonoptimized) and 88%, respectively (Scheme 4). The reaction conditions for the radiosynthesis of [^{18}F]3f and [^{18}F]3h closely resembled those of the well-known oncological PET tracer 2-[^{18}F]fluoro-2-deoxyglucose (FDG),⁵² and the workup procedure consisted of only one HPLC purification step. Thus, the radiosynthesis of [^{18}F]3h resulted in a decay-uncorrected RCY of 22% (related to [^{18}F]fluoride) within a total synthesis time of only 60 min, which is most favorable when compared with the decay-uncorrected RCY at end of synthesis of the respective radioligands (^{18}F]3a–f, Table 4). All radioligands were isolated by semipreparative HPLC and formulated in phosphate-buffered solution to determine $\log D_{7.4}$ values and to study their in vitro stability in human serum at 37 °C. The radiochemical purity of all radioligands was >98% and the specific activity was 24–47 GBq/ μmol (starting from relatively low amounts of [^{18}F]fluoride, i.e., 0.6–1.2 GBq).

Lipophilicity. As a marker of lipophilicity, experimental $\log D_{7.4}$ values of all tested radioligands ranged from 1.78 to 2.15, reflecting mainly the influence of the partly protonated piperazine at pH 7.4 (Table 4). However, calculated $\log P$ values obtained by the software cLogP (Biobyte) revealed values of 1.9 for the pyridinyl compounds [^{18}F]3a and [^{18}F]3c, and $\log P$ values of 2.9 for the [^{18}F]fluoroethoxy-substituted radioligands [^{18}F]3e, [^{18}F]3f, and [^{18}F]3h (Table 4). Due to the fact that radiotracer uptake in the brain has been determined to be a function of $\log P$ that peaks between $\log P$ of 2 and 3,⁵³ the $\log P$ values of our tested ^{18}F -labeled pyrazolo[1,5-*a*]pyridine-based D_4 radioligands excellently complied with this requirement. Moreover, the tested radioligands revealed high stability in human serum, even after long-term incubation for up to 90 min (Table 4). These in vitro parameters could suggest advantageous in vivo characteristics, such as adequate blood–brain barrier penetration. This assumption is supported by our previous in vivo studies on structurally related compounds,^{36,54} confirm-

ing the ability of **10** and 7-iodo-**9** to adequately cross the blood–brain barrier.

In Vitro Autoradiography. Due to the superior D_4 R subtype selectivity together with the convenient and high-yielding radiosynthesis, we chose the inverse agonist radioligand [^{18}F]3h to perform in vitro autoradiography studies on native tissue. The results of the in vitro autoradiography using coronal rat brain slices are presented in Figure 3. All brain areas were determined by histological counterstaining of each slice and verification of the brain regions with reference to the rat brain atlas of Paxinos and Watson.⁵⁵ In the slices representing total binding (Figure 3A,F), increased uptake values of [^{18}F]3h were detected in the brain areas of the gyrus dentate region of the hippocampus, the hypothalamus (HT), the medial habenular nucleus (MHb), the central medial thalamic nucleus (CM), septum (s), and cortex (CX) (Figure 3). Interestingly, total binding in the area of the striatum (ST) was low in comparison with the surrounding cortex (Figure 3F). Importantly, the D_4 -selective ligand **10**³⁴ (Figure 3C,H) and also the nonselective dopamine receptor antagonist eticlopride (Figure 3D,I) significantly inhibited the binding of [^{18}F]3h in the brain regions under investigation by 78–93% ($n = 9$) and 65–80% ($n = 7$), respectively, as determined by integration of regions of interest (ROI). This result suggested specific binding of [^{18}F]3h in the above-mentioned areas of the rat brain. Together with low binding in the striatum, the observed in vitro binding pattern of [^{18}F]3h excellently reflects the published D_4 receptor expression in rat brain that had been determined by D_4 R antibody staining and autoradiography with [^3H]NGD 94-1.^{6–8} However, Primus et al. observed additional binding sites in the subregions CA1, CA2, and CA3 of the rat hippocampus by [^3H]NGD 94-1 autoradiography,⁶ whereas we exclusively observed specific uptake of [^{18}F]3h in the gyrus dentate of the hippocampus and only background levels of [^{18}F]3h uptake in CA1–3. This discrepancy could be due to tissue-specific differences in intrinsic efficacy and receptor content being responsible for differences in partial agonist ([^3H]NGD 94-1)¹¹ and inverse agonist ([^{18}F]3h) binding potency between the subregions of the hippocampus.

To provide a “gold standard” of a selective “ D_4 radioligand” for comparison with [^{18}F]3h binding, we performed rat brain autoradiography using [^3H]nemonapride as a high affinity unselective D_2 , D_3 , and D_4 radioligand supplemented with 1 μM cold raclopride to block D_2 and D_3 receptors (Figure 3E). This method has been used previously for quantitative analysis of the dopamine D_4 receptor in the mouse brain.¹⁴ As shown in Figure 3E, specific [^3H]nemonapride binding excellently correlated with brain areas of high specific binding of [^{18}F]3h (cf. Figure 3A), thus suggesting accurate localization of D_4 receptors by [^{18}F]3h in the gyrus dentate of the hippocampus, the hypothalamus (HT), the medial habenular nucleus (MHb), the central medial thalamic nucleus (CM), and the cortex (CX). However, in comparison with [^{18}F]3h and similar to [^3H]NGD 94-1,⁶ [^3H]nemonapride revealed additional binding sites in CA1–3 of the hippocampus that did not show specific binding of [^{18}F]3h. Interfering nondopaminergic and nonserotonergic binding sites of [^3H]nemonapride (1 μM raclopride) in the striatum of D_4 R knockout mice have been noticed previously.¹⁴ This suggests that [^{18}F]3h could represent a D_4 radioligand with improved selectivity compared to the system [^3H]nemonapride/cold raclopride, possibly due to the inverse agonist properties of [^{18}F]3h.

In summary, [^{18}F]3h is a promising D_4 radioligand candidate for PET due to its convenient radiosynthesis, superior D_4 R

Table 4. Reaction Conditions of the ¹⁸F-Syntheses of [¹⁸F]3a, [¹⁸F]3c, [¹⁸F]3e, [¹⁸F]3f, and [¹⁸F]3h and the Corresponding Radiochemical Yields (RCY), Experimental log D_{7.4} Values and In Vitro Stability in Human Serum^a

labeling precursor	¹⁸ F-labeling conditions	product	decay-corrected RCY (%)	RCY at EOS (%)	serum stability ^b (%)	log D _{7.4} (exp.)	cLogP ^c
3b	[¹⁸ F]fluoride, DMSO,	[¹⁸ F]3a	69 ± 8	13 ± 4	>98	1.98 ± 0.14	1.9
3d	180 °C, 45–60 min	[¹⁸ F]3c	80 ± 2 ^d	5 ± 1	>99	1.78 ± 0.04	1.9
7a	2-[¹⁸ F]fluoroethyltosylate,	[¹⁸ F]3e	92 ± 7	15 ± 3	nd	2.15 ± 0.03	2.9
7b	NaOMe, DMF, 120 °C, 5 min	[¹⁸ F]3f	87 ± 5	12 ± 3	>96	2.12 ± 0.13	2.9
8a	[¹⁸ F]fluoride, CH ₃ CN,	[¹⁸ F]3f	26 ± 7 ^e	<10 ^e			
8b	85 °C, 10 min	[¹⁸ F]3h	88 ± 4	22 ± 2	>99	1.99 ± 0.06	2.9

^a Data are expressed as mean ± SD of 3–9 experiments. RCY = radiochemical yield. EOS = end of synthesis. ^b Intact radioligand after incubation in human serum at 37 °C for 90 min. ^c Calculated using the cLogP software (Biobyte Corp.). ^d Maximum value. ^e Nonoptimized RCY; nd = not determined.

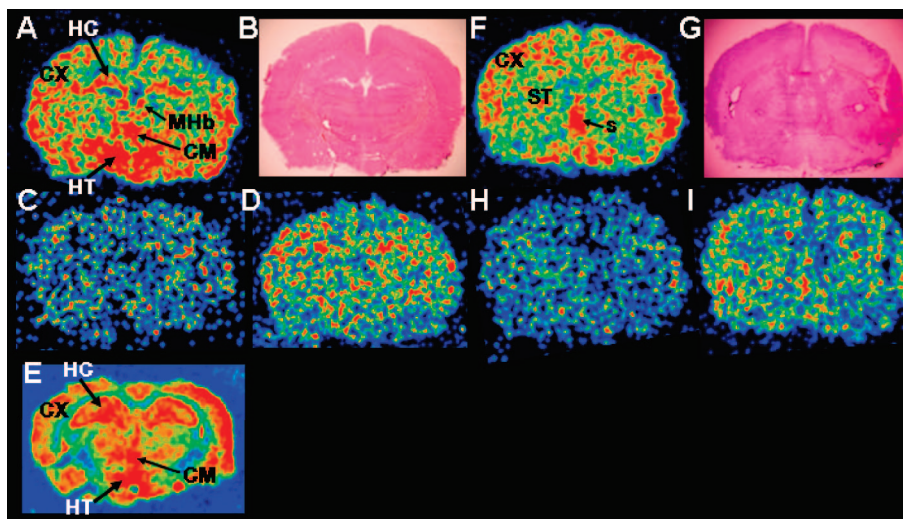


Figure 3. In vitro autoradiography of [¹⁸F]3h and histological counterstaining of rat brain coronal slices (20 μm; level of hippocampus, B; level of striatum, G). Total binding (A) in the area of the hippocampus (HC; that is gyrus dentate of HC only), hypothalamus (HT), cortex (CX), medial habenular nucleus (MHb), and central medial thalamic nucleus (CM), was inhibited by the D₄-selective antagonist **10** (1 μM; C) and by the nonselective dopamine receptor–ligand eticlopride (1 μM; D). In slices at the level of the rat striatum (F–I) specific binding in the cortex (CX) and septum (s), and negligible binding in the striatum (ST) was detected (F). Again, binding of [¹⁸F]3h was inhibited by the D₄ selective antagonist **10** (1 μM; G) and by eticlopride (1 μM; H). (E) Autoradiogram at the level of the hippocampus obtained by incubation with 1 nM [³H]nemonapride in the presence of 1 μM cold raclopride as a reference (please note that HC staining is positive for CA1, CA2, CA3, and gyrus dentate of HC).

subtype selectivity, high serum stability, relatively low lipophilicity, and encouraging in vitro rat brain autoradiography and, thus, could also be suitable for the observation of a D₄ receptor-specific signal in vivo. However, the in vitro receptor affinity measured by a cell-based assay was not exceptionally high (13 nM, Table 1), and the specific activity of [¹⁸F]3h was relatively low, suggesting that meaningful imaging of the apparently low D₄ receptor densities in vivo might be problematic. In this context, it should be noted that data on rat brain D₄ receptor densities are scarce and the target site of inverse D₄ agonists has not yet been explored neither in vitro nor in vivo. Thus, little is known about tissue-specific differences in intrinsic efficacy and receptor content that determine the in vivo binding potential (B_{max}/K_d)⁵⁶ of an inverse agonist D₄R radioligand for PET. Besides high in vivo receptor affinity, parameters such as blood–brain barrier permeability, metabolic stability, and “functional selectivity” of inverse agonist candidates, such as [¹⁸F]3h, could additionally influence the in vivo specificity of a PET D₄R radioligand. Further biodistribution studies are currently in progress to characterize the in vivo specificity of [¹⁸F]3h as a selective inverse agonist PET radioligand for the D₄ receptor.

Conclusion

We reported the syntheses, binding affinities, functional characterization, ¹⁸F-radiosyntheses, and in vitro studies of selective pyrazolo[1,5-*a*]pyridine-based D₄ receptor ligands. All

radioligands had favorable log *P* values and showed high serum stability. [¹⁸F]3h revealed an outstanding subtype selectivity for the D₄ receptor and could be obtained by a high-yielding straightforward radiosynthesis that allows easy automation for further routine radiopharmaceutical production. In vitro autoradiography studies using rat brain slices suggest specific binding of [¹⁸F]3h in brain areas that are in agreement with the known D₄R distribution. Thus, [¹⁸F]3h (FAUC F41) represents a potential radioligand for the exploration of D₄ receptor densities in vivo by PET.

Experimental Section

No-carrier-added (n.c.a.) [¹⁸F]fluoride was produced by the ¹⁸O(p,n)¹⁸F reaction on ¹⁸O-enriched (95%) water using a proton beam of 11 MeV generated by a RDS 111 cyclotron (PET Net GmbH, Erlangen, Germany). Solid-phase cartridges (Sep-PakPlus C18 cartridges) were purchased from Waters (Eschborn, Germany). Melting points (mp) were uncorrected and obtained with a Mel-TempII apparatus (Laboratory Devices, MA, U.S.A.). Thin layer chromatography (TLC) was carried out on silica gel-coated aluminum plates (silica gel/TLC-cards, with fluorescent indicator 254 nm, 0.2 mm, Fluka). Radio-TLC was performed with silica gel coated plastic sheets (Polygram, Sil G/UV₂₅₄, Macherey-Nagel). Radio-HPLC was performed on the following system: Agilent 1100 with a quaternary pump and variable wavelength (VWL) detector and radio-HPLC-detector (D505TR, Canberra Packard). Each ¹⁸F-labeled compound was identified by retention time (*t_R*) on the radio-HPLC system and coinjection of the corresponding reference compound. NMR spectra were recorded on a Bruker Avance 360

or Bruker Avance 600 using TMS as internal standard, and data are reported as follows: chemical shifts (ppm), multiplicity (s, singlet; d, doublet; t, triplet; q, quartet; br, broad; m, multiplet), peak integral. LC-MS analyses were performed on an Agilent 1100 Series analytic HPLC system with a VWL detector coupled to a Bruker esquire 2000 mass spectrometer with atmospheric pressure chemical ionization (APCI). High resolution mass spectrometry (HRMS) was performed on a JEOL JMS-GC Mate II spectrometer. 1-(2-(2-Fluoroethoxy)phenyl)piperazine (**1c**), 1-(4-(2-fluoroethoxy)phenyl)piperazine (**1d**), and 4-(4-hydroxyphenyl)piperazine-1-carboxylic acid *t*-butyl ester (**4c**) were synthesized as described previously.³⁹ Pyrazolo[1,5-*a*]pyridine (**2a**) was prepared as reported by Löber et al.³⁴ 4-(6-Bromopyridin-2-yl)piperazine-1-carboxylic acid *t*-butyl ester (**4b**), 1-(2-hydroxyphenyl)piperazine (**4d**), and 1-(4-hydroxyphenyl)piperazine (**4e**) were purchased from Sigma-Aldrich.

General Procedure. Preparation of 3-[4-Arylpiperazin-1-ylmethyl]pyrazolo[1,5-*a*]pyridine Derivatives (3a, 3b, 3e, 3f, 7a, 7b, 8a). A solution of **2a** (0.3–0.7 mmol, 1 equiv), the corresponding arylpiperazine (**1a–d**, **4d**, **4e**, or **6**, 1 equiv), acetic acid (0.26 mL), and formaldehyde (50 μ L, 37% in H₂O) in CH₂Cl₂ (5 mL) was stirred at room temperature (6 h or overnight). The reaction was quenched by the addition of aqueous saturated NaHCO₃ (10 mL). The solution was extracted with CH₂Cl₂ (3 \times 10 mL), and the combined organic phases were dried (Na₂SO₄). The solvent was evaporated in vacuo and the residue was purified by silica gel column chromatography (CH₂Cl₂/methanol, 95:5).

3-[4-(6-Fluoropyridin-2-yl)piperazin-1-ylmethyl]pyrazolo[1,5-*a*]pyridine (3a). Obtained from **1a** (79 mg, 0.66 mmol) as a white solid (45 mg, 0.14 mmol, 22%). Mp 112 °C. TLC (CH₂Cl₂/methanol, 95:5): *R*_f = 0.37. ¹H NMR (CDCl₃, 600 MHz): δ 2.54–2.70 (m, 4H), 3.53–3.66 (m, 4H), 3.82 (s, 2H), 6.16 (dd, *J* = 7.7 Hz, *J* = 2.7 Hz, 1H, 5-H (pyridyl)), 6.39 (dd, *J* = 8.2 Hz, *J* = 2.4 Hz, 1H, 3-H (pyridyl)), 6.77 (dd (t), *J* = 6.6 Hz, 1H, 6-H), 7.13 (dd (t), *J* = 8.0 Hz, 1H, 5-H), 7.51 (ddd (q), *J* = 8.2 Hz, 1H, 4-H (pyridyl)), 7.66 (brd, *J* = 8.8 Hz, 1H, 4-H), 7.93 (s, 1H, 2-H), 8.45 (d, *J* = 7.0 Hz, 1H, 7-H). LC-MS (APCI): *m/z* 312.4 [M + H]⁺.

3-[4-(6-Bromopyridin-2-yl)piperazin-1-ylmethyl]pyrazolo[1,5-*a*]pyridine (3b). Obtained from **1b** (26.7 mg, 0.11 mmol) as a dark yellow solid (37 mg, 0.10 mmol, 91%). Mp 98 °C. TLC (CH₂Cl₂/MeOH 95:5): *R*_f = 0.47. ¹H NMR (CDCl₃, 360 MHz): δ 2.55–2.60 (m, 4H), 3.53–3.59 (m, 4H), 3.77 (s, 2H), 6.47 (d, *J* = 8.3 Hz, 1H), 6.73 (d, *J* = 7.5 Hz, 1H), 6.75 (ddd (dt), *J* = 6.9 Hz, *J* = 1.3 Hz, 1H), 7.11 (ddd, *J* = 8.9 Hz, *J* = 6.7 Hz, *J* = 1.0 Hz, 1H), 7.26 (dd, *J* = 8.4 Hz, *J* = 7.5 Hz, 1H), 7.63 (brd, *J* = 8.9 Hz, 1H), 7.91 (s, 1H, 2-H), 8.44 (ddd (dt), *J* = 7.0 Hz, *J* = 1.0 Hz, *J* = 1.0 Hz, 1H). LC-MS (APCI): *m/z* 374.0 [M + H]⁺.

3-[4-(2-(2-Fluoroethoxy)phenyl)piperazin-1-ylmethyl]pyrazolo[1,5-*a*]pyridine (3e). Obtained from **1c** (74 mg, 0.33 mmol) as a stringy yellow oil (19.3 mg, 0.05 mmol, 16%). TLC (CH₂Cl₂/methanol, 95:5): *R*_f = 0.23. ¹H NMR (CDCl₃, 600 MHz): δ 2.67 (m, 4H), 3.12 (m, 4H), 3.77 (s, 2H), 4.25 (dt, *J* = 28.1 Hz, *J* = 4.1 Hz, 2H, OCH₂), 4.76 (dt, *J* = 47.5 Hz, *J* = 4.2 Hz, 2H, FCH₂), 6.74 (ddd (dt), *J* = 6.8 Hz, *J* = 1.2 Hz, 1H), 6.87–6.83 (m, 1H), 6.98–6.91 (m, 3H), 7.10 (ddd, *J* = 8.9 Hz, *J* = 6.7 Hz, *J* = 0.9 Hz, 1H), 7.64 (brd, *J* = 8.9 Hz, 1H), 7.92 (s, 1H, 2-H), 8.43 (d, *J* = 7.0 Hz, 1H). LC-MS (APCI): *m/z* 355.1 [M + H]⁺, 225.1 [C₁₂H₁₇FN₂O + H]⁺, 131.0 [C₈H₇N₂ + H]⁺.

3-[4-(4-(2-Fluoroethoxy)phenyl)piperazin-1-ylmethyl]pyrazolo[1,5-*a*]pyridine (3f). Obtained from **1d** (73 mg, 0.33 mmol) as a white solid after crystallization from methanol (50 mg, 0.14 mmol, 31%). Mp 131 °C. TLC (CH₂Cl₂/methanol, 95:5): *R*_f = 0.28. ¹H NMR (CDCl₃, 600 MHz): δ 2.61–2.68 (m, 4H), 3.08–3.13 (m, 4H), 3.77 (s, 2H), 4.16 (dt, *J* = 27.9 Hz, *J* = 4.2 Hz, 2H, OCH₂), 4.72 (dt, *J* = 47.4 Hz, *J* = 4.3 Hz, 2H, FCH₂), 6.75 (dd (t), *J* = 6.4 Hz, 1H), 6.83–6.89 (m, 4H), 7.10 (dd (t), *J* = 8.27 Hz, 1H), 7.64 (d, *J* = 8.9 Hz, 1H), 7.91 (s, 1H), 8.44 (d, *J* = 7.0 Hz, 1H). LC-MS (APCI): *m/z* 355.2 [M + H]⁺, 131.0 [C₈H₇N₂ + H]⁺.

3-[4-(2-Hydroxyphenyl)piperazin-1-ylmethyl]pyrazolo[1,5-*a*]pyridine (7a). Obtained from 1-(2-hydroxyphenyl)piperazine (**4d**, 121 mg, 0.68 mmol) as a white solid (145 mg, 0.47 mmol, 69%). Mp 129 °C. TLC (CH₂Cl₂/methanol, 95:5): *R*_f = 0.35. ¹H NMR (CDCl₃, 600 MHz): δ 2.52–2.81 (m, 4H), 2.87–2.94 (m, 4H), 3.79 (s, 2H), 6.76 (dd (t), *J* = 6.7 Hz, 1H, 6-H), 6.85 (ddd (dt), *J* = 7.7 Hz, *J* = 7.7 Hz, *J* = 1.4 Hz, 1H), 6.93 (dd, *J* = 8.0 Hz, *J* = 1.4 Hz, 1H), 7.06 (ddd (dt), *J* = 8.0 Hz, *J* = 8.0 Hz, *J* = 1.5 Hz, 1H), 7.13 (brdd (t), *J* = 7.5 Hz, 1H, 5-H), 7.16 (dd, *J* = 7.9 Hz, *J* = 1.4 Hz, 1H), 7.64 (brd, *J* = 8.9 Hz, 1H, 4-H), 7.93 (s, 1H, 2-H), 8.45 (d, *J* = 7.0 Hz, 1H, 7-H).

3-[4-(4-Hydroxyphenyl)piperazin-1-ylmethyl]pyrazolo[1,5-*a*]pyridine (7b). Obtained from 1-(4-hydroxyphenyl)piperazine (**4e**, 121 mg, 0.68 mmol) as a white solid (139 mg, 0.45 mmol, 67%). Mp 173.5 °C. TLC (CH₂Cl₂/methanol, 95:5): *R*_f = 0.26. ¹H NMR (CDCl₃, 600 MHz): δ 2.65 (m, 4H), 3.09 (m, 4H), 3.78 (s, 2H), 6.73–6.75 (m, 3H), 6.80–6.85 (m, 2H), 7.11 (brdd (t), *J* = 7.6 Hz, 1H, 5-H), 7.64 (brd, *J* = 8.7 Hz, 1H, 4-H), 7.92 (s, 1H, 2-H), 8.44 (brd, *J* = 7.0 Hz, 1H, 7-H).

3-[4-(4-(2-Tosylethoxy)phenyl)piperazin-1-ylmethyl]pyrazolo[1,5-*a*]pyridine (8a). Obtained from **6** as a yellow oil (54 mg, 0.11 mmol, 40%). TLC (CH₂Cl₂/methanol, 95:5): *R*_f = 0.28. ¹H NMR (CDCl₃, 360 MHz): δ 2.44 (s, 3H), 2.63–2.68 (m, 4H), 3.07–3.11 (m, 4H), 3.78 (s, 2H), 4.07–4.10 (m, 2H), 4.30–4.34 (m, 2H), 6.71 (d, *J* = 9.2 Hz, 2H), 6.75 (ddd (dt), *J* = 6.9 Hz, *J* = 6.9 Hz, *J* = 1.4 Hz, 1H, 6-H), 6.82 (d, *J* = 9.2 Hz, 2H), 7.10 (ddd, *J* = 8.9 Hz, *J* = 6.7 Hz, *J* = 1.1 Hz, 1H, 5-H), 7.33 (d, *J* = 8.6 Hz, 2H), 7.63 (ddd (dt), *J* = 8.9 Hz, *J* = 1.2 Hz, *J* = 1.2 Hz, 1H, 4-H), 7.81 (d, *J* = 8.3 Hz, 2H), 7.91 (s, 1H, 2-H), 8.44 (ddd (dt), *J* = 7.0 Hz, *J* = 1.0 Hz, *J* = 1.0 Hz, 1H, 7-H). LC-MS (APCI): *m/z* 507.3 [M + H]⁺, 377.2 [C₁₉H₂₄N₂O₄ + H]⁺, 131.0 [C₈H₇N₂ + H]⁺.

General Procedure. Preparation of 2-[4-Arylpiperazin-1-ylmethyl]pyrazolo[1,5-*a*]pyridine Derivatives (3c, 3d, 3g, 3h, 7c). Compound **2b** (1 equiv) and the corresponding arylpiperazine (**1a–d**, **6**, 1 equiv) were dissolved in anhydrous CH₂Cl₂. Na(OAc)₃BH (3 equiv) was added and the mixture was stirred at room temperature (24 h). The reaction was quenched by the addition of saturated NaHCO₃ (20 mL) and the solution was extracted with CH₂Cl₂ (3 \times 10 mL). The organic layer was dried (Na₂SO₄) and evaporated to dryness. The crude product was purified by silica gel column chromatography using CH₂Cl₂/methanol (95:5) as eluent.

2-[4-(6-Fluoropyridin-2-yl)piperazin-1-ylmethyl]pyrazolo[1,5-*a*]pyridine (3c). Obtained from **1a** as a brownish solid (59 mg, 0.19 mmol, 57%). Mp 118 °C. TLC (CH₂Cl₂/methanol, 95:5): *R*_f = 0.34. ¹H NMR (DMSO-*d*₆, 360 MHz): δ 2.52–2.55 (m, 4H), 3.44–3.49 (m, 4H), 3.71 (s, 2H), 6.24 (dd, *J* = 7.7 Hz, *J* = 2.8 Hz, 1H, 5-H (pyridyl)), 6.53 (s, 1H, 3-H), 6.65 (dd, *J* = 8.2 Hz, *J* = 2.7 Hz, 1H, 3-H (pyridyl)), 6.82 (ddd (dt), *J* = 6.8 Hz, *J* = 6.8 Hz, *J* = 1.4 Hz, 1H, 6-H), 7.17 (ddd, *J* = 8.9 Hz, *J* = 6.7 Hz, *J* = 1.1 Hz, 1H, 5-H), 7.59–7.68 (m, 2H, 4-H, 4-H (pyridyl)), 8.59 (dd, *J* = 7.0 Hz, *J* = 1.0 Hz, 1H, 7-H). LC-MS (APCI): *m/z* 312.3 [M + H]⁺.

2-[4-(6-Bromopyridin-2-yl)piperazin-1-ylmethyl]pyrazolo[1,5-*a*]pyridine (3d). Obtained from **1b** as a white solid (159 mg, 0.42 mmol, 35%). Mp 106 °C. TLC (CH₂Cl₂/methanol, 95:5): *R*_f = 0.50. ¹H NMR (DMSO-*d*₆, 360 MHz): δ 2.51–2.55 (m, 4H), 3.45–3.50 (m, 4H), 3.70 (s, 2H), 6.53 (s, 1H, 3-H), 6.77 (d, *J* = 7.4 Hz, 1H, pyridyl), 6.78 (d, *J* = 8.4 Hz, 1H, pyridyl), 6.82 (ddd (dt), *J* = 6.8 Hz, *J* = 6.8 Hz, *J* = 1.4 Hz, 1H, 6-H), 7.17 (ddd, *J* = 8.9 Hz, *J* = 6.7 Hz, *J* = 1.1 Hz, 1H, 5-H), 7.42 (dd, *J* = 8.4 Hz, *J* = 7.4 Hz, 1H, 4-H (pyridyl)), 7.61 (ddd (dt), *J* = 8.9 Hz, *J* = 1.2 Hz, *J* = 1.2 Hz, 1H, 4-H), 8.59 (ddd, *J* = 7.0 Hz, *J* = 1.0 Hz, *J* = 1.0 Hz, 1H, 7-H). LC-MS (APCI): *m/z* 374.0 [M + H]⁺, 244.0 [C₉H₁₂BrN₃ + H]⁺.

2-[4-(2-(2-Fluoroethoxy)phenyl)piperazin-1-ylmethyl]pyrazolo[1,5-*a*]pyridine (3g). Obtained from **1c** as a pale yellow oil (22 mg, 0.06 mmol, 29%). TLC (CH₂Cl₂/methanol, 95:5): *R*_f = 0.26. ¹H NMR (CDCl₃, 360 MHz): δ 2.77 (m, 4H), 3.17 (m, 4H), 3.83 (s, 2H), 4.25 (dt, *J* = 28.0 Hz, *J* = 4.2 Hz, 2H, OCH₂), 4.76 (dt, *J* = 47.4 Hz, *J* = 4.2 Hz, 2H, FCH₂), 6.51 (s, 1H), 6.70 (ddd

(dt), $J = 6.9$ Hz, $J = 1.4$ Hz, 1H), 6.85 (ddd, $J = 7.1$, $J = 3.7$, $J = 1.4$ Hz, 1H), 6.93–6.97 (m, 3H), 7.07 (ddd, $J = 8.90$, $J = 6.7$ Hz, $J = 1.1$ Hz, 1H), 7.47 (ddd, $J = 8.9$ Hz, $J = 1.2$ Hz, $J = 1.2$ Hz, 1H), 8.42 (ddd, $J = 7.1$ Hz, $J = 2.0$ Hz, $J = 1.0$ Hz, 1H). LC-MS (APCI): m/z 355.2 [M + H]⁺.

2-[4-(4-(2-Fluoroethoxy)phenyl)piperazin-1-ylmethyl]pyrazolo[1,5-*a*]pyridine (3h). Obtained from **1d** as a pale yellow oil (30.6 mg, 0.09 mmol, 57%). TLC (CH₂Cl₂/methanol, 95:5): $R_f = 0.21$. ¹H NMR (CDCl₃, 360 MHz): δ 3.40 (brs, 8H), 4.16 (dt, $J = 27.8$ Hz, $J = 4.2$ Hz, 2H, OCH₂), 4.51 (s, 2H), 4.72 (dt, $J = 47.4$ Hz, $J = 4.2$ Hz, 2H, FCH₂), 6.76 (s, 1H, 3-H), 6.83–6.93 (m, 5H), 7.19 (dd, $J = 8.9$ Hz, $J = 6.8$ Hz, 1H, 5-H), 7.58 (brd, $J = 8.8$ Hz, 1H, 4-H), 8.44 (brd, $J = 6.6$ Hz, 1H, 7-H). LC-MS (APCI): m/z 355.3 [M + H]⁺.

2-[4-(4-Hydroxyphenyl)piperazin-1-ylmethyl]pyrazolo[1,5-*a*]pyridine (7c). Obtained from 1-(4-hydroxyphenyl)piperazine (**4e**) as a white solid (77.5 mg, 0.25 mmol, 52%). TLC (CH₂Cl₂/methanol, 95:5): $R_f = 0.35$. ¹H NMR (CDCl₃, 600 MHz): δ 2.75 (brs, 4H), 3.13 (brs, 4H), 3.84 (brs, 2H), 6.50 (s, 1H, 3-H), 6.72 (dd (t), $J = 7.0$ Hz, 1H, 6-H), 6.75 (d, $J = 9.0$ Hz, 2H), 6.84 (d, $J = 8.9$ Hz, 2H), 7.08 (dd (t), $J = 7.7$ Hz, 1H, 5-H), 7.47 (brd, $J = 8.9$ Hz, 1H, 4-H), 8.42 (dd, $J = 7.0$ Hz, $J = 0.9$ Hz, 1H, 7-H). LC-MS (APCI): m/z 309.2 [M + H]⁺.

2-[4-(4-(2-Tosylethoxy)phenyl)piperazin-1-ylmethyl]pyrazolo[1,5-*a*]pyridine (8b). Compound **8b** was prepared following the synthetic protocol for **5**. Starting from **7c** (95 mg, 0.31 mmol), ethylene glycol-1,2-ditosylate (342 mg, 0.92 mmol) and potassium carbonate (25 mg, 0.18 mmol) gave **8b** as a pale yellow oil (58 mg, 0.12 mmol, 37%). TLC (CH₂Cl₂/methanol, 95:5): $R_f = 0.29$. ¹H NMR (CDCl₃, 360 MHz): δ 2.44 (s, 3H), 2.69–2.82 (m, 4H), 3.01–3.15 (m, 4H), 3.82 (s, 2H), 4.06–4.10 (m, 2H), 4.31–4.36 (m, 2H), 6.49 (brs, 1H, 3-H), 6.70 (ddd (dt), $J = 6.9$ Hz, $J = 6.9$ Hz, $J = 1.4$ Hz, 1H, 6-H), 6.71 (d, $J = 9.2$ Hz, 2H), 6.83 (d, $J = 9.2$ Hz, 2H), 7.07 (ddd, $J = 8.9$ Hz, $J = 6.7$ Hz, $J = 1.1$ Hz, 1H, 5-H), 7.30–7.35 (m, 2H), 7.47 (brd, $J = 8.9$ Hz, 1H, 4-H), 7.78–7.83 (m, 2H), 8.42 (ddd, $J = 7.0$ Hz, $J = 2.1$ Hz, $J = 1.1$ Hz, 1H, 7-H). LC-MS (APCI): m/z 507.5 [M + H]⁺.

Radiochemistry. 3-[4-(6-[¹⁸F]Fluoropyridin-2-yl)piperazin-1-ylmethyl]pyrazolo[1,5-*a*]pyridine (¹⁸F]3a). No-carrier-added [¹⁸F]fluoride (400–800 MBq) was eluted from a QMA-cartridge with a solution of Kryptofix 2.2.2 (15 mg) and K₂CO₃ (15 μ L, 1 M) in acetonitrile/water (8:2, 1 mL). The solution was evaporated using a stream of nitrogen at 85 °C and coevaporated to dryness with CH₃CN (2 \times 200 μ L). A solution of **3b** (5.6 mg, 15 μ mol) in anhydrous DMSO (0.5 mL) was added at 180 °C. The progression of the reaction was analyzed by radio-HPLC. The radiochemical yield of [¹⁸F]3a was 69 \pm 8% after 45 min, as determined by radio-HPLC from a sample withdrawn from the reaction mixture (Lichrosorb RP18, 250 \times 4.6 mm, 1 mL/min, linear gradient from 25% to 100% CH₃CN in water (0.1% TFA) over 30 min; $t_R = 7.38$ min). The reaction mixture was diluted with water (0.5 mL) and passed through a C18-cartridge (Sep-PakPlus, Waters), washed with water (10 mL), and eluted with acetonitrile (1.5 mL) in a reaction vessel. The solvent was evaporated and the residue was dissolved in acetonitrile/water (2:3 v/v, 0.5 mL) for injection on a semipreparative HPLC system. [¹⁸F]3a was isolated by semipreparative reversed-phase HPLC (Lichrosorb RP18, 125 \times 8 mm, 4 mL/min, CH₃CN/H₂O (30/70; 0.1% TFA)). The fraction containing [¹⁸F]3a was diluted with water (1:10) and the radiolabeled product was fixed on a RP18-cartridge (100 mg, Merck). The cartridge was dried in a nitrogen stream and eluted with acetonitrile (1 mL). The solvent was evaporated in vacuo and [¹⁸F]3a (52–104 MBq) was formulated in phosphate-buffered saline (PBS, 0.3 mL) for further experimental use. Starting from [¹⁸F]fluoride (400–800 MBq), the decay-uncorrected radiochemical yield of [¹⁸F]3a was 13 \pm 4% ($n = 3$, based on [¹⁸F]fluoride) after a total synthesis time of 95 min.

2-[4-(6-[¹⁸F]Fluoropyridin-2-yl)piperazin-1-ylmethyl]pyrazolo[1,5-*a*]pyridine (¹⁸F]3c). The radiosynthesis of [¹⁸F]3c was accomplished in a manner identical to [¹⁸F]3a, using precursor **3d** (5.6 mg, 15 μ mol) dissolved in anhydrous DMSO (0.5 mL). The

maximum radiochemical yield of [¹⁸F]3c was 80 \pm 2% after 60 min at 180 °C. The decay-uncorrected radiochemical yield of [¹⁸F]3c averaged 5 \pm 1% ($n = 3$, based on [¹⁸F]fluoride) after a total synthesis time of 110 min. Radio-HPLC (Lichrosorb RP18, 250 \times 4.6 mm, 1 mL/min, linear gradient from 25% to 100% CH₃CN in water (0.1% TFA) over 30 min): $t_R = 8.12$ min.

3-[4-(2-(2-[¹⁸F]Fluoroethoxy)phenyl)piperazin-1-ylmethyl]pyrazolo[1,5-*a*]pyridine (¹⁸F]3e). A solution of **7a** (2.3 mg, 7.5 μ mol) in anhydrous DMF (250 μ L) and sodium methanolate (50 μ L, 0.15 μ M in dry methanol) were stirred for 3 min at 120 °C under nitrogen. 1-[¹⁸F]Fluoro-2-tosyloxyethane^{39,51} (140–250 MBq) in dry DMF (250 μ L) were added, and the progression of the reaction was analyzed by radio-TLC (CH₂Cl₂/methanol 95:5). The radiochemical yield of [¹⁸F]3e was 92 \pm 7% after 5 min at 120 °C. Radio-HPLC (Lichrosorb RP18, 250 \times 4.6 mm, 1 mL/min, linear gradient from 30% to 70% methanol in water (0.1% TFA) over 30 min): $t_R = 17.8$ min. The reaction was quenched by the addition of water (4.5 mL) and the solution was passed through a C18-cartridge (Sep-PakPlus, Waters). The cartridge was washed with water (10 mL), dried in a stream of nitrogen, and eluted with CH₃CN (1 mL). The solution was subjected to a semipreparative HPLC column (Lichrosorb RP-18, 125 \times 8 mm, 4 mL/min, CH₃CN/H₂O, 40/60 (0.1% TFA)). The [¹⁸F]3e containing fraction was diluted with water (1:10 v/v) and the product was fixed on a RP18-cartridge (100 mg, Merck), dried in a nitrogen stream and eluted with CH₃CN (1 mL). The solvent was evaporated and [¹⁸F]3e was formulated in PBS (300 μ L). [¹⁸F]3e (39–65 MBq) was obtained in a decay-uncorrected yield of 13 \pm 3% (related to [¹⁸F]fluoride) after a total synthesis time of 120 min.

3-[4-(4-(2-[¹⁸F]Fluoroethoxy)phenyl)piperazin-1-ylmethyl]pyrazolo[1,5-*a*]pyridine (¹⁸F]3f). Variation A: [¹⁸F]3f was synthesized by ¹⁸F-fluoroethylation as described for [¹⁸F]3e using **7b** (2.5 mg, 16 μ mol) as the labeling precursor and 1-[¹⁸F]fluoro-2-tosyloxyethane in the presence of sodium methanolate in DMF/methanol (550 μ L, 9:1 v/v). The radiochemical yield of [¹⁸F]3f was 87 \pm 5% after 5 min at 120 °C as determined by radio-HPLC (Lichrosorb RP18, 250 \times 4.6 mm, 1 mL/min, linear gradient from 30 to 70% methanol in water (0.1% TFA) over 30 min): $t_R = 17.0$ min). The workup procedure, including semipreparative HPLC, was performed as described for [¹⁸F]3e. [¹⁸F]3f was obtained in a decay-uncorrected yield of 12 \pm 3% after a total synthesis time of 120 min.

Variation B: [¹⁸F]3f was synthesized by direct nucleophilic substitution with no-carrier-added [¹⁸F]fluoride in a Kryptofix 2.2.2-promoted reaction as described above (see [¹⁸F]3a). A solution of **8a** (6 mg, 12 μ mol) in anhydrous CH₃CN (0.5 mL) was added to a reaction vessel containing the dried [K⁺222]⁺[¹⁸F][−] complex and the reaction mixture was stirred at 85 °C. The progression of the reaction was analyzed by radio-HPLC. The radiochemical yield of [¹⁸F]3f was 26 \pm 7% ($n = 4$) after 10 min as determined by radio-HPLC from a sample withdrawn from the reaction mixture (Kromasil C8, 250 \times 4.6 mm, 1 mL/min, linear gradient from 30 to 100% CH₃CN in water (0.1% TFA) over 30 min): $t_R = 9.13$ min). The workup procedure including semipreparative HPLC was performed as described for [¹⁸F]3h. Starting from [¹⁸F]fluoride (300–800 MBq), [¹⁸F]3f was obtained in a decay-uncorrected yield of <10% after a total synthesis time of about 60 min. Variation B was used to obtain PBS-formulated [¹⁸F]3f for the determination of serum stability.

2-[4-(2-(2-[¹⁸F]Fluoroethoxy)phenyl)piperazin-1-ylmethyl]pyrazolo[1,5-*a*]pyridine (¹⁸F]3h). No-carrier-added [¹⁸F]fluoride (600–1200 MBq) was eluted from a QMA-cartridge and the drying process was performed as described above. A solution of **8b** (6.1 mg, 12 μ mol) in anhydrous CH₃CN (0.5 mL) was added to the dried kryptate ([K⁺222]⁺[¹⁸F][−]) and the reaction mixture was stirred at 85 °C. The progression of the reaction was analyzed by radio-HPLC. The radiochemical yield of [¹⁸F]3h was 88 \pm 4% ($n = 3$) after 10 min as determined by radio-HPLC from a sample withdrawn from the reaction mixture (Kromasil C8, 250 \times 4.6 mm, 1 mL/min, linear gradient of 30 to 100% CH₃CN in water (0.1% TFA) over 30 min): $t_R = 9.63$ min). The reaction was quenched

by the addition of water (10 mL) and the solution was passed through a C18-cartridge (Sep-PakPlus, Waters), washed with water (5 mL), and eluted with CH₃CN (1.5 mL). [¹⁸F]3h was purified with HPLC on a Kromasil C-8 column (125 × 8 mm, 4 mL/min, CH₃CN/H₂O, 30/70 (0.1% TFA)). [¹⁸F]3h (*t*_R = 4.85 min) was collected, concentrated by solid-phase extraction (RP18-cartridge, 100 mg, Merck), and eluted with ethanol (1 mL). The solvent was removed by evaporation and [¹⁸F]3h (130–270 MBq) was formulated in PBS (300 μL). The decay-uncorrected radiochemical yield of [¹⁸F]3h averaged 22 ± 2% (*n* = 9, based on [¹⁸F]fluoride) after a total synthesis time of 60 min and the specific activity was >40 GBq/μmol as determined by radio-HPLC with monitoring UV absorbance at 254 nm using authentic 3h as a reference.

Receptor Binding Experiments. Receptor binding experiments were performed, as described previously.⁴⁴ Briefly, the dopamine D₁ receptor assay was done with porcine striatal membranes (40 μg/assay tube) and at 0.3 nM [³H]SCH23390 (*K*_d = 0.5 nM). Competition experiments with the human D_{2long}, D_{2short}, D₃, and D_{4.4} receptors were performed using preparations of membranes from CHO cells stably expressing the corresponding receptor (6–30 μg/assay tube) and [³H]spiperone at a final concentration of 0.5 nM. The obtained *K*_d values for [³H]spiperone were of 0.10 nM for D_{2long}, D_{2short}, and D₃ and 0.10–0.13 nM for D_{4.4}. Serotonin 5-HT_{1A}, 5-HT₂, and adrenergic α₁ binding were measured utilizing porcine cortical membranes and the selective radioligands [³H]8-OH-DPAT, [³H]ketanserin, and [³H]prazosin, respectively, each at a final concentration of 0.5 nM. The resulting competition curves were analyzed by nonlinear regression using the algorithm in PRISM (GraphPad Software, San Diego, U.S.A.). The data were fitted using the sigmoid model to provide IC₅₀ values, which were transformed to *K*_i values according to the equation of Cheng and Prusoff.⁵⁷

Mitogenesis Assay. The mitogenesis experiments were performed with a CHO10001A cell line stably transfected with the rat dopamine D_{4.2} receptor.⁵⁸ In brief, cells were grown in MEM α-medium supplemented with fetal calf serum (FCS), L-glutamine, penicillin G, streptomycin, and hygromycin B at 37 °C under a humidified atmosphere of 5% CO₂ at a density of 10000 cells/well. After 72 h, the growth medium was removed and the cells were rinsed twice with serum-free medium. Incubation was started by the addition of seven different concentrations of each test compound (with a final concentration of 0.01–10000 nM) diluted in sterile water (10 μL) to each well containing serum-free medium (90 μL). Eight wells of every plate contained 100 μL serum-free medium or medium supplemented with 10% FCS to control stimulation of growth. After incubation for 20 h, [³H]thymidine (0.02 μCi, specific activity = 25 Ci/mmol) in serum-free medium (10 μL) was added to each well and incubation was proceeded for 2 h at 37 °C. Finally, cells were trypsinized and harvested onto GF/C filters using an automated cell harvester. Filters were washed four times with ice-cold PBS buffer and counted in a microplate scintillation counter.

Determination of Partition Coefficient (log *D*_{7.4}). The lipophilicity of ¹⁸F-labeled radioligands was assessed by determination of the water–octanol partition coefficient following the procedure described previously.⁵⁴ 1-Octanol (0.5 mL) was added to a solution of approximately 25 kBq of the ¹⁸F-labeled compound in PBS (0.5 mL, pH 7.4) and the layers were vigorously mixed for 3 min at room temperature. The tubes were centrifuged (3000 rpm, 10 min) and three samples of 100 μL of each layer were counted in a gamma counter (Wallac Wizard). The partition coefficient was determined by calculating the ratio cpm (octanol)/cpm (PBS) and expressed as log *D*_{7.4} = log(cpm_{octanol}/cpm_{buffer}). For each test ligand, 2–3 independent experiments were performed in triplicate and data were provided as mean values ± standard deviation.

Stability in Human Serum. The serum stability of ¹⁸F-labeled compounds was evaluated by incubation in human serum at 37 °C for up to 90 min. An aliquot of the PBS-formulated ¹⁸F-labeled compound (20 μL, 250 MBq/mL) was added to a sample of human serum (200 μL), and the mixture was incubated at 37 °C. Samples of 10 μL each were taken after designated periods (10–90 min) and quenched in methanol/CH₂Cl₂ (1:1 v/v, 100 μL) followed by

centrifugation for 3 min. The organic layer was analyzed by radio-TLC using CH₂Cl₂/methanol (95:5). In some cases, an aliquot of the organic layer (10 μL) was evaporated to dryness under reduced pressure and the residue was dissolved in water/CH₃CN (1:1 v/v, 50 μL) for radio-HPLC analysis.

In Vitro Autoradiography of Rat Brain Slices. Rat brain slices were prepared from Sprague–Dawley rats according to protocols approved by the local Animal Protection Authorities (Regierung Mittelfranken, Germany, No. 54-2531.31-28/06). Female Sprague–Dawley rats (200–240 g) were housed in groups of 2–3 in individual cages in a temperature- and air-controlled room with free access to food and water (Franz–Penzoldt Center, Erlangen). Animals were maintained on a 12 h light/dark cycle before experimental use. Autoradiography of rat brain slices was performed following the procedure of Zhang et al.⁵⁹ with slight modifications. Sprague–Dawley rats were sacrificed by decapitation and brains were removed and frozen in cooled hexane at –70 °C. Coronal brain sections (20 μm) were cut on a cryostat microtome (HM550, Microm, Germany) and thaw-mounted on covered glass slides (Histobond). The brain slices were carefully dried at room temperature and preincubated for 2 × 5 min (50 mM Tris-HCl, 120 mM NaCl, 1 mM EDTA, 5 mM MgCl₂, pH 7.4). The sections were incubated at room temperature for 60 min in assay buffer (50 mM Tris-HCl, 120 mM NaCl, 1 mM EDTA, 5 mM MgCl₂, 0.5 μM 1,3-di-*o*-tolyguanidine (DTG, sigma receptor agonist), 0.1 μM pindolol (serotonin receptor antagonist), pH 7.4) containing 110 kBq/mL [¹⁸F]3h in the presence and absence of eticlopride (1 μM) or 10 (1 μM), respectively. Coronal brain sections of the same level of the hippocampus were preincubated, as described, and incubation with 1 nM [³H]nemonapride (D₂, D₃, D₄ radioligand, obtained from Perkin-Elmer, specific activity 82.7 Ci/mmol) in the presence of 1 μM raclopride, to block D₂ and D₃ receptors, was performed using the assay buffer, as described above. Nonspecific binding was measured in the presence of 60 μM sulpiride. Subsequently, slices were washed two times for 5 min in fresh cold assay buffer and dipped briefly in ice-cold distilled water. The slices were dried under a slight stream of air. The brain slices were then covered by a solid scintillator sheet for real-time autoradiography (*μ*-Imager, Biospace). ¹⁸F radioactivity measurements were started within 2 h after incubation with a duration of 15 min for each slice. The duration of ³H radioactivity measurements was 48 h. After ¹⁸F autoradiography, conventional HE staining of the same sections was performed, allowing definition of regions of interest (ROIs) referring to the rat brain atlas of Paxinos and Watson.⁵⁵ The ROIs were then transferred to the autoradiograms for determination of intensities (cpm/mm²) within each brain region using the software provided by the manufacturer (Beta-Vision Software, Biospace).

Acknowledgment. The authors thank Professor Dr. Ingmar Blümcke (Institute of Neuropathology, Erlangen) for his expert support in the anatomical determination of rat brain regions and Mrs. Bianca Weigel for technical assistance. We thank Dr. J.-C. Schwartz and Dr. P. Sokoloff (INSERM, Paris), Dr. J. Shine (The Garvan Institute of Medical Research, Sydney) and the late Dr. H. H. M. Van Tol (Clarke Institute of Psychiatry, Toronto) for providing D₃, D₂, and D_{4.4} receptor expressing cell lines, respectively, and Dr. R. M. Huff (Pfizer, Kalamazoo, MI) for providing D_{4.2} receptor expressing cells. We gratefully acknowledge Wilhelm Hamkens, Marco Pschierer, and Jan Kubin (PET Net GmbH, Erlangen) for producing and delivering [¹⁸F]fluoride and for excellent collaboration. This work was supported by the Deutsche Forschungsgemeinschaft (DFG, PR 677/2-1 and PR 677/2-2).

Supporting Information Available: Experimental procedures and analytical data for compounds 1a,b, 2b, 4a, 5, and 6, and tabulated HPLC and HRMS data for compounds 3a–3h, 7a, 7b, and 8b. This material is available free of charge via the Internet at <http://pubs.acs.org>.

References

- (1) Neve, K. A.; Neve, R. L. *The Dopamine Receptors*; Humana Press: Totowa, NJ, 1997.
- (2) Sokoloff, P.; Schwartz, J. C. Novel dopamine receptors half a decade later. *Trends Pharmacol. Sci.* **1995**, *16*, 270–275.
- (3) Stanwood, G. D.; Artymyshyn, R. P.; Kung, M. P.; Kung, H. F.; Lucki, I.; McGonigle, P. Quantitative autoradiographic mapping of rat brain dopamine D₃ binding with [¹²⁵I]7-OH-PIPAT: Evidence for the presence of D₃ receptors on dopaminergic and nondopaminergic cell bodies and terminals. *J. Pharmacol. Exp. Ther.* **2000**, *295*, 1223–1231.
- (4) Van Tol, H. H.; Bunzow, J. R.; Guan, H. C.; Sunahara, R. K.; Seeman, P.; Niznik, H. B.; Civelli, O. Cloning of the gene for a human dopamine D₄ receptor with high affinity for the antipsychotic clozapine. *Nature* **1991**, *350*, 610–614.
- (5) Ariano, M. A.; Wang, J.; Noblett, K. L.; Larson, E. R.; Sibley, D. R. Cellular distribution of the rat D-4 dopamine receptor protein in the CNS using anti-receptor antisera. *Brain Res.* **1997**, *752*, 26–34.
- (6) Primus, R. J.; Thurkauf, A.; Xu, J.; Yevich, E.; McInerney, S.; Shaw, K.; Tallman, J. F.; Gallager, D. W. Localization and characterization of dopamine D₄ binding sites in rat and human brain by use of the novel, D₄ receptor-selective ligand [³H]NGD 94-1. *J. Pharmacol. Exp. Ther.* **1997**, *282*, 1020–1027.
- (7) Defagot, M. C.; Malchiodi, E. L.; Villar, M. J.; Antonelli, M. C. Distribution of D₄ dopamine receptor in rat brain with sequence-specific antibodies. *Mol. Brain Res.* **1997**, *45*, 1–12.
- (8) Khan, Z. U.; Gutierrez, A.; Martin, R.; Penafiel, A.; Rivera, A.; De La Calle, A. Differential regional and cellular distribution of dopamine D₂-like receptors: An immunocytochemical study of subtype-specific antibodies in rat and human brain. *J. Comp. Neurol.* **1998**, *402*, 353–371.
- (9) Noain, D.; Avale, M. E.; Wedemeyer, C.; Calvo, D.; Peper, M.; Rubinstein, M. Identification of brain neurons expressing the dopamine D₄ receptor gene using BAC transgenic mice. *Eur. J. Neurosci.* **2006**, *24*, 2429–2438.
- (10) Tallman, J. F.; Primus, R. J.; Brodbeck, R.; Cornfield, L.; Meade, R.; Woodruff, K.; Ross, P.; Thurkauf, A.; Gallager, D. W. NGD 94-1: Identification of a novel, high-affinity antagonist at the human dopamine D₄ receptor. *J. Pharmacol. Exp. Ther.* **1997**, *282*, 1011–1019.
- (11) Gazi, L.; Sommer, B.; Nozulak, J.; Schoeffter, P. NGD 94-1 as an agonist at human recombinant dopamine D_{4.4} receptors expressed in HEK293 cells. *Eur. J. Pharmacol.* **1999**, *372*, R9–10.
- (12) Tarazi, F. I.; Kula, N. S.; Baldessarini, R. J. Regional distribution of dopamine D₄ receptors in rat forebrain. *NeuroReport* **1997**, *8*, 3423–3426.
- (13) Defagot, M. C.; Antonelli, M. C. Autoradiographic localization of the putative D₄ dopamine receptor in rat brain. *Neurochem. Res.* **1997**, *22*, 401–407.
- (14) Defagot, M. C.; Falzone, T. L.; Low, M. J.; Grandy, D. K.; Rubinstein, M.; Antonelli, M. C. Quantitative analysis of the dopamine D₄ receptor in the mouse brain. *J. Neurosci. Res.* **2000**, *59*, 202–208.
- (15) Ebstein, R. P. The molecular genetic architecture of human personality: beyond self-report questionnaires. *Mol. Psychiatry* **2006**, *11*, 427–445.
- (16) Melis, M. R.; Succu, S.; Mascia, M. S.; Argiolas, A. PD-168077, a selective dopamine D-4 receptor agonist, induces penile erection when injected into the paraventricular nucleus of male rats. *Neurosci. Lett.* **2005**, *379*, 59–62.
- (17) Succu, S.; Sanna, F.; Melis, T.; Boi, A.; Argiolas, A.; Melis, M. R. Stimulation of dopamine receptors in the paraventricular nucleus of the hypothalamus of male rats induces penile erection and increases extra-cellular dopamine in the nucleus accumbens: Involvement of central oxytocin. *Neuropharmacology* **2007**, *52*, 1034–1043.
- (18) Seeman, P.; Guan, H. C.; Van Tol, H. H. Dopamine D₄ receptors elevated in schizophrenia. *Nature* **1993**, *365*, 441–445.
- (19) Oak, J. N.; Oldenhof, J.; Van Tol, H. H. M. The dopamine D-4 receptor: One decade of research. *Eur. J. Pharmacol.* **2000**, *405*, 303–327.
- (20) Wong, A. H. C.; Van Tol, H. H. M. The dopamine D-4 receptors and mechanisms of antipsychotic atypicality. *Prog. Neuropsychopharmacol. Biol. Psych.* **2003**, *27*, 1091–1099.
- (21) Lee, C. M.; Farde, L. Using positron emission tomography to facilitate CNS drug development. *Trends Pharmacol. Sci.* **2006**, *27*, 310–316.
- (22) Elsinga, P. H.; Hatano, K.; Ishiwata, K. PET tracers for imaging of the dopaminergic system. *Curr. Med. Chem.* **2006**, *13*, 2139–2153.
- (23) Zhang, A.; Neumeyer, J. L.; Baldessarini, R. J. Recent progress in development of dopamine receptor subtype-selective agents: Potential therapeutics for neurological and psychiatric disorders. *Chem. Rev.* **2007**, *107*, 274–302.
- (24) Hertel, P.; Didriksen, M.; Pouzet, B.; Brennum, L. T.; Soby, K. K.; Larsen, A. K.; Christoffersen, C. T.; Ramirez, T.; Marcus, M. M.; Svensson, T. H.; Di Matteo, V.; Esposito, E.; Bang-Andersen, B.; Arnt, J. Lu 35-138 ((+)-(S)-3-{1-[2-(1-acetyl-2,3-dihydro-1H-indol-3-yl)ethyl]-3,6-dihydro-2H-pyridin-4-yl}-6-chloro-1H-indole), a dopamine D₄ receptor antagonist and serotonin reuptake inhibitor: Characterisation of its in vitro profile and pre-clinical antipsychotic potential. *Eur. J. Pharmacol.* **2007**, *573*, 148–160.
- (25) Chemel, B. R.; Roth, B. L.; Armbruster, B.; Watts, V. J.; Nichols, D. E. WAY-100635 is a potent dopamine D₄ receptor agonist. *Psychopharmacology (Berlin)* **2006**, *188*, 244–251.
- (26) Newman-Tancredi, A.; Assie, M. B.; Martel, J. C.; Cosi, C.; Slot, L. B.; Palmier, C.; Raully-Lestienne, I.; Colpaert, F.; Vacher, B.; Cussac, D. F15063, a potential antipsychotic with D₂/D₃ antagonist, 5-HT_{1A} agonist and D₄ partial agonist properties. I. In vitro receptor affinity and efficacy profile. *Br. J. Pharmacol.* **2007**, *151*, 237–252.
- (27) Boy, C.; Klimke, A.; Holschbach, M.; Herzog, H.; Mühlensiepen, H.; Kops, E. R.; Sonnenberg, F.; Gaebel, W.; Stöcklin, G.; Markstein, R.; Müller-Gärtner, H. W. Imaging dopamine D-4 receptors in the living primate brain: A positron emission tomography study using the novel D-1/D-4 antagonist C-11 SDZ GLC 756. *Synapse* **1998**, *30*, 341–350.
- (28) Langer, O.; Halldin, C.; Chou, Y. H.; Sandell, J.; Swahn, C. G.; Nagren, K.; Perrone, R.; Berardi, F.; Leopoldo, M.; Farde, L. Carbon-11 PB-12: An attempt to visualize the dopamine D₄ receptor in the primate brain with positron emission tomography. *Nucl. Med. Biol.* **2000**, *27*, 707–714.
- (29) Zhang, M. R.; Haradahira, T.; Maeda, J.; Okauchi, T.; Kawabe, K.; Noguchi, J.; Kida, T.; Suzuki, K.; Sahara, T. Syntheses and pharmacological evaluation of two potent antagonists for dopamine D-4 receptors: [¹¹C]YM-50001 and N-[2-[4-(4-chlorophenyl)-piperazin-1-yl]ethyl]-3-[¹¹C]methoxybenzamide. *Nucl. Med. Biol.* **2002**, *29*, 233–241.
- (30) Matarrese, M.; Soloviev, D.; Moresco, R. M.; Todde, S.; Simonelli, P.; Colombo, D.; Magni, F.; Carpinelli, A.; Fazio, F.; Kienle, M. G. Synthesis and in vivo evaluation of 3-[¹¹C]methyl-(3-methoxynaphthalen)-2-yl-(1-benzyl-piperidin)-4-yl-acetate (SB-235753), as a putative dopamine D-4 receptors antagonist for PET. *J. Labelled Compd. Radiopharm.* **2000**, *43*, 359–374.
- (31) Eskola, O.; Bergman, J.; Lehtikoinen, P.; Haaparanta, M.; Gronroos, T.; Forsback, S.; Solin, O. Synthesis of 3-[[4-(4-[¹⁸F]fluorophenyl)piperazin-1-yl]methyl]-1H-pyrrolo[2,3-b]pyridine. *J. Labelled Compd. Radiopharm.* **2002**, *45*, 687–696.
- (32) Oh, S. J.; Lee, K. C.; Lee, S. Y.; Ryu, E. K.; Saji, H.; Choe, Y. S.; Chi, D. Y.; Kim, S. E.; Lee, J.; Kim, B. T. Synthesis and evaluation of fluorine-substituted 1H-pyrrolo[2,3-b]pyridine derivatives for dopamine D₄ receptor imaging. *Bioorg. Med. Chem. Lett.* **2004**, *12*, 5505–5513.
- (33) Löber, S.; Hübner, H.; Gmeiner, P. Azaindole derivatives with high affinity for the dopamine D₄ receptor: Synthesis, ligand binding studies and comparison of molecular electrostatic potential maps. *Bioorg. Med. Chem. Lett.* **1999**, *9*, 97–102.
- (34) Löber, S.; Hübner, H.; Utz, W.; Gmeiner, P. Rationally based efficacy tuning of selective dopamine D₄ receptor ligands leading to the complete antagonist 2-[4-(4-chlorophenyl)piperazin-1-yl]methylpyrazolo[1,5-a]pyridine (FAUC 213). *J. Med. Chem.* **2001**, *44*, 2691–2694.
- (35) Löber, S.; Hübner, H.; Gmeiner, P. Synthesis and biological investigations of dopaminergic partial agonists preferentially recognizing the D₄ receptor subtype. *Bioorg. Med. Chem. Lett.* **2006**, *16*, 2955–2959.
- (36) Boeckler, F.; Russig, H.; Zhang, W.; Löber, S.; Schetz, J.; Hübner, H.; Ferger, B.; Gmeiner, P.; Feldon, J. FAUC 213, a highly selective dopamine D₄ receptor full antagonist, exhibits atypical antipsychotic properties in behavioural and neurochemical models of schizophrenia. *Psychopharmacology (Berlin)* **2004**, *175*, 7–17.
- (37) Prante, O.; Löber, S.; Hübner, H.; Gmeiner, P.; Kuwert, T. Synthesis and in vitro evaluation of iodine labelled pyrazolo[1,5-a]pyridines as highly selective dopamine D₄ receptor ligands. *J. Labelled Compd. Radiopharm.* **2001**, *44*, 849–858.
- (38) Hocke, C.; Prante, O.; Löber, S.; Hübner, H.; Gmeiner, P.; Kuwert, T. Synthesis and evaluation of ¹⁸F-labeled dopamine D₃ receptor ligands as potential PET imaging agents. *Bioorg. Med. Chem. Lett.* **2005**, *15*, 4819–4823.
- (39) Tietze, R.; Hocke, C.; Löber, S.; Hübner, H.; Kuwert, T.; Gmeiner, P.; Prante, O. Syntheses and radiofluorination of two derivatives of 5-cyano-indole as selective ligands for the dopamine subtype-4 receptor. *J. Labelled Compd. Radiopharm.* **2006**, *49*, 55–70.
- (40) Salama, I.; Hocke, C.; Utz, W.; Prante, O.; Boeckler, F.; Hübner, H.; Kuwert, T.; Gmeiner, P. Structure–selectivity investigations of D₂-like receptor ligands by CoMFA and CoMSIA guiding the discovery of D₃ selective PET radioligands. *J. Med. Chem.* **2007**, *50*, 489–500.

- (41) Hayes, G.; Biden, T. J.; Selbie, L. A.; Shine, J. Structural subtypes of the dopamine D2 receptor are functionally distinct: expression of the cloned D2A and D2B subtypes in a heterologous cell line. *Mol. Endocrinol.* **1992**, *6*, 920–926.
- (42) Sokoloff, P.; Giros, B.; Martres, M. P.; Bouthenet, M. L.; Schwartz, J. C. Molecular cloning and characterization of a novel dopamine receptor (D3) as a target for neuroleptics. *Nature* **1990**, *347*, 146–151.
- (43) Asghari, V.; Sanyal, S.; Buchwaldt, S.; Paterson, A.; Jovanovic, V.; Vantol, H. H. M. Modulation of intracellular cyclic-Amp levels by different human dopamine D4 receptor variants. *J. Neurochem.* **1995**, *65*, 1157–1165.
- (44) Hübner, H.; Haubmann, C.; Utz, W.; Gmeiner, P. Conjugated enynes as nonaromatic catechol bioisosteres: Synthesis, binding experiments, and computational studies of novel dopamine receptor agonists recognizing preferentially the D₃ subtype. *J. Med. Chem.* **2000**, *43*, 756–762.
- (45) Chio, C. L.; Lajiness, M. E.; Huff, R. M. Activation of heterologously expressed D3 dopamine receptors: comparison with D2 dopamine receptors. *Mol. Pharmacol.* **1994**, *45*, 51–60.
- (46) de Ligt, R. A.; Kourounakis, A. P.; AP, I. J. Inverse agonism at G protein-coupled receptors: (patho)physiological relevance and implications for drug discovery. *Br. J. Pharmacol.* **2000**, *130*, 1–12.
- (47) Kenakin, T. Inverse, protean, and ligand-selective agonism: Matters of receptor conformation. *FASEB J.* **2001**, *15*, 598–611.
- (48) Burstein, E. S.; Ma, J.; Wong, S.; Gao, Y.; Pham, E.; Knapp, A. E.; Nash, N. R.; Olsson, R.; Davis, R. E.; Hacksell, U.; Weiner, D. M.; Brann, M. R. Intrinsic efficacy of antipsychotics at human D2, D3, and D4 dopamine receptors: Identification of the clozapine metabolite *N*-desmethylclozapine as a D2/D3 partial agonist. *J. Pharmacol. Exp. Ther.* **2005**, *315*, 1278–1287.
- (49) Strange, P. G. Antipsychotic drugs: importance of dopamine receptors for mechanisms of therapeutic actions and side effects. *Pharmacol. Rev.* **2001**, *53*, 119–133.
- (50) Wang, H.-E.; Wu, S.-Y.; Chang, C.-W.; Liu, R.-S.; Hwang, L.-C.; Lee, T.-W.; Chen, J.-C.; Hwang, J.-J. Evaluation of F-18-labeled amino acid derivatives and [¹⁸F]FDG as PET probes in a brain tumor-bearing animal model. *Nucl. Med. Biol.* **2005**, *32*, 367–375.
- (51) Block, D.; Coenen, H. H.; Stöcklin, G. The N. C. A. nucleophilic ¹⁸F-fluorination of 1-*N*-disubstituted alkanes as fluoroalkylation agents. *J. Labelled Compd. Radiopharm.* **1987**, *24*, 1029–1042.
- (52) Hamacher, K.; Coenen, H. H.; Stöcklin, G. Efficient stereospecific synthesis of no-carrier-added 2-[¹⁸F]-fluoro-2-deoxy-D-glucose using aminopolyether supported nucleophilic substitution. *J. Nucl. Med.* **1986**, *27*, 235–238.
- (53) Waterhouse, R. N. Determination of lipophilicity and its use as a predictor of blood–brain barrier penetration of molecular imaging agents. *Mol. Imaging Biol.* **2003**, *5*, 376–389.
- (54) Prante, O.; Hocke, C.; Löber, S.; Hübner, H.; Gmeiner, P.; Kuwert, T. Tissue distribution of radioiodinated FAUC113—Assessment of a pyrazolo[1,5-*a*]pyridine-based dopamine D4 receptor radioligand candidate. *Nuklearmedizin* **2006**, *45*, 41–48.
- (55) Paxinos, G.; Watson, C. *The Rat Brain in Stereotaxic Coordinates*; Academic Press, Inc.: San Diego, 1986.
- (56) Eckelman, W. C.; Mathis, C. A. Targeting proteins in vivo: In vitro guidelines. *Nucl. Med. Biol.* **2006**, *33*, 161–164.
- (57) Cheng, Y.-C.; Prusoff, W. H. Relationship between the inhibition constant (*K*_i) and the concentration of inhibitor which causes 50% inhibition (*I*₅₀) of an enzymatic reaction. *Biochem. Pharmacol.* **1973**, *22*, 3099–3108.
- (58) Hübner, H.; Kraxner, J.; Gmeiner, P. Cyanoindole derivatives as highly selective dopamine D₄ receptor partial agonists: Solid-phase synthesis, binding assays, and functional experiments. *J. Med. Chem.* **2000**, *43*, 4563–4569.
- (59) Zhang, K.; Weiss, N. T.; Tarazi, F. I.; Kula, N. S.; Baldessarini, R. J. Effects of alkylating agents on dopamine D₃ receptors in rat brain: selective protection by dopamine. *Brain Res.* **1999**, *847*, 32–37.

JM701375U